LANGMUIR

Subscriber access provided by UNIV OF DURHAM

Biological and Environmental Phenomena at the Interface

Hierarchical rose-petal surfaces delay the early-stage bacterial biofilm growth

yunyi cao, Saikat Jana, Leon Bowen, Xiaolong Tan, Hongzhong Liu, Nadia Rostami, James Brown, Nicholas S. Jakubovics, and Jinju Chen

Langmuir, **Just Accepted Manuscript** • DOI: 10.1021/acs.langmuir.9b02367 • Publication Date (Web): 20 Oct 2019

Hierarchical rose-petal surfaces delay the early-stage bacterial biofilm growth

Yunyi Cao[†], Saikat Jana[†], Leon Bowen[‡], Xiaolong Tan[ℓ], Hongzhong Liu[§], Nadia Rostami[ǂ], James Brown[#], Nicholas S. Jakubovics[ǂ] and Jinju Chen[†]*

[†] School of Engineering, Newcastle University, Newcastle Upon Tyne, NE1 7RU, UK; [‡] Department of Physics, Durham University, Durham, DH1 3LE, UK; [ℓ] School of Pharmacy, Newcastle University, Newcastle Upon Tyne, NE1 7RU, UK; [§] School of Mechanical Engineering, Xi'an Jiaotong University, Xi'an 710054;. [ǂ] School of Dental Sciences, Newcastle University, Newcastle Upon Tyne, NE2 4BW, UK; [#]Centre for Biomolecular Sciences, University of Nottingham, Nottingham, NG7 2RD, UK.

ABSTRACT

A variety of natural surfaces exhibit antibacterial properties; as a result significant efforts in the past decade have been dedicated towards fabrication of biomimetic surfaces that can help control biofilm growth. Examples of such surfaces include rose petals, which possess hierarchical structures like the micro-papillae measuring tens of microns and nano-folds that range in the size of 700 ±100 nm. We duplicated the natural structures on rose-petal surfaces via a simple UV-curable nanocasting technique, and tested the efficacy of these artificial surfaces in preventing biofilm growth using clinically relevant bacteria strains. The rose-petal structured surfaces exhibited hydrophobicity (contact angle~130.8º ±4.3º) and high contact angle hysteresis (~91.0° ±4.9°). Water droplets on rose-petal replicas evaporated following the constant contact line mode, indicating the likely coexistence of both Cassie and Wenzel states (Cassie-Baxter impregnating wetting state). Fluorescent microscopy and image analysis

revealed the significantly lower attachment of *Staphylococcus epidermidis* (86.1± 6.2% less) and *Pseudomonas aeruginosa* (85.9 ±3.2% less) on the rose-petal structured surfaces, compared with flat surfaces over a period of 2 hours. Extensive biofilm matrix was observed in biofilms formed by both species on flat surfaces after prolonged growth (several days), but was less apparent on rose-petal biomimetic surfaces. In addition, the biomass of *S. epidermidis* (63.2 ±9.4% less) and *P. aeruginosa* (76.0 ±10.0% less) biofilms were significantly reduced on the rose-petal structured surfaces, in comparison to the flat surfaces. By comparing *P. aeruginosa* growth on representative unitary nano-pillars, we demonstrated that hierarchical structures are more effective in delaying biofilm growth. The mechanisms are two-fold: 1) the nano-folds across the hemispherical micro-papillae restrict initial attachment of bacterial cells and delay the direct contacts of cells via cell alignment, and 2) the hemispherical micro-papillae arrays isolate bacterial clusters and inhibit the formation of a fibrous network. The hierarchical features on rose petal surfaces may be useful for developing strategies to control biofilm formation in medical and industrial contexts.

1. INTRODUCTION

Bacteria are ubiquitous in the environment and can adhere onto abiotic or biotic surfaces to form biofilms[1]. These three-dimensional (3D) communities of sessile cells are encased in a matrix of extracellular polymeric substances (EPS). Biofilms can be useful in biotechnological processes such as bioremediation, biofertilizers, and in microbial fuel cells[1]. By contrast, certain biofilms can be detrimental to human health, causing infections and diseases[1-2]. It has been estimated that up to 80% of bacterial infections in humans are biofilm associated, and biofilms are responsible for the majority of hospital-acquired infections. Biofilm associated infections are the fourth leading cause of death worldwide, within the U.S. about 2 million annual cases lead to more than $5 billion USD in added medical costs per annum[3-5]. In the UK, about 300,000 people per annum in England suffer from hospital-acquired infections under NHS care and the costs also run into billions of pounds[6]. Hence, it is important to investigate techniques that can control biofilm growth and reduce the instances of infections. Bacterial biofilms are robust structures and are difficult to treat via traditional antibiotic therapy[5-7]. The EPS matrix acts as a barrier to agents trying to access the interior of the biofilm, subsequently triggering the development of antibiotic resistance[7], which has been shown for both *Staphylococcus epidermidis*[5] and *Pseudomonas aeruginosa*[8]. Physical strategies, in particular the use of rationally designed surface topographies, have gained interests and present us with

an interesting approach to prevent bacterial adherence and biofilm growth without the requirement for antimicrobials[9-10].

Natural surfaces with micro/nano topographical patterns have inspired researchers to design artificial biomimetic surfaces to control biofilm growth. For example, lotus leaf has hierarchical structures such as micro-papillae (measuring ~3–11 μm diameter) that are randomly covered by nano-tubules (~100 nm diameter)[11-12]. Water droplets on these surfaces cannot penetrate the air pockets formed within the hierarchical structures (i.e. Cassie state)[11-12]. As a result the lotus leaf is found to exhibit superhydrophobicity with a contact angle (CA) >150° and a low contact angle hysteresis (CAH) (i.e. <10°), which results in the easy rolling off of water droplets (i.e. self-cleaning effects) [12-14]. However, it is challenging to reproduce the hierarchical structures on lotus leaf in the laboratory[15-17]. Using lotus leaf as a template, it has only been possible to fabricate unitary structures based on the micro-papillae; the nano-tubules are too small for this approach[18-23]. Hierarchical structures similar to the lotus leaf can be generated using chemical processes, but these are not exactly the same structures as found on natural lotus leaves[24-27]. Nevertheless, lotus leaf-inspired superhydrophobic surfaces (unitary structure or hierarchical structures) can mitigate biofouling by a range of bacteria including *Staphylococcus aureus*, *S. epidermidis*, *P. aeruginosa* and *Planococcus maritimus*, since the trapped air restricts the direct contact between the solid surfaces and micro-orgasisms[18, 20-21]. The anti-fouling efficacy strongly depends on the lifetime of non-wetting (Cassie) state. The wetting transition (Cassie to Wenzel state) can occur within 1-4 hours in submerged environments, with a significant decrease in CA and increase in CAH[10, 18]. Bacteria can also accelerate such transitions, for example by flagella-mediated motility[10]. Therefore, it is commonly accepted that surface topography features such as size, pitch or height play a primary role in delaying bacterial attachment or biofilm growth and that wettability (CA and CAH) is less important, especially when surfaces get fully wetted[5, 10, 20, 28].

Different surface topographies on many other natural surfaces including rice leaves[29], shark-skin[30-32], gecko-skin[9, 33-34], cicada wings[5, 35-36], or dragonfly wings[37-38] have also been demonstrated to have anti-biofilm properties to different levels. Topographical features larger than bacterial cells, such as the microstructures in Sharklet AF™, constrain bacterial deposition to recessed regions and delay biofilm formation[32]. Topographies close in size to bacteria can lead to alignment of rod-shaped bacterial cells between the surface features and retard biofilm formation, possibly by blocking cell-cell communications[39-42]. By contrast, features such as tightly-spaced nano-spears that are smaller than bacterial cells can delay surface attachment

without necessarily restricting biofilm formation to a great extent [5, 10]. Previous investigations have reported that rose petals have hierarchical structures with micro-papillae (~20 µm diameter) and nano-sized cuticular folds (~730 nm width)[43-44]. Such hierarchical structures make the rose-petal surface superhydrophobic even allowing it to exert a high adhesive force on droplets[43]. A few studies examined the dynamics of water droplets and efficacy of the structured surfaces in preventing bacterial growth[43-44]. However, the mechanism responsible for the inhibition of bacterial growth by the rose-petal structures is not well-understood. There was also lack of study about how such structures may affect bacteria alignment and biofilm formation.

The present study focuses on investigating bacterial attachment and early-stage biofilm formation on biomimetic rose-petal surfaces. The imprints of rose-petal hierarchical structures were fabricated via nanocasting technique. The wettability of rose-petal replicas were accessed by the static/dynamic contact angle measurement and droplet evaporation tests. By using fluorescent microscopy and scanning electron microscope (SEM), growth of two clinically relevant biofilm forming strains *S. epidermidis* and *P. aeruginosa* were evaluated on the rose-petal-structured and flat surfaces. In addition, by comparing the growth of *P. aeruginosa* on the model unitary nano-pillar structures, we demonstrated the efficacy of hierarchical structures in delaying biofilm growth.

2. MATERIALS AND METHODS

2.1 Surface fabrication: One piece of fresh rose petal (Figure 1a) was attached to a glass slide (1 cm ×1 cm) via a double-sided adhesive tape (Figure 1b). A mixture of Poly(dimethylsiloxane) (PDMS) and its curing agent was prepared from SYLGARD 184 Elastomer Kit (Dow Corning Corporation, Midland, MI) with a ratio of 10:1 (wt/wt). The solution was thoroughly mixed and degassed in a vacuum chamber for 30 minutes to eliminate air bubbles. The mixture was poured over the glass slide with rose petals in a Petri dish (Figure 1c), and cured at room temperature for 48 hours. After curing, the PDMS mould was gently peeled off which left a negative imprint of the structures on the petal (Figure 1d). UV-curable epoxy (OG 142-87, Epoxy Technology, Inc.) was poured onto the negative imprint of the PDMS mould and was gently covered with a pre-cleaned glass slide (1 cm ×1 cm) as a substrate. The UV-curable epoxy was cured under a UV-lamp, with the luminous intensity of 100 mW/cm^2 and the

wavelength of 365 nm, for 20–25 minutes until fully cured (Figure 1e). After cooling to room temperature, the cured epoxy was demoulded by bending the PDMS mould (Figure 1f).

To better understand the advantage of the hierarchical structures over the unitary structures, a similar technique was used to produce periodic nano-pillar structures (diameter ~500 nm, pitch ~1 µm, height ~2 µm) with the same materials. More details can be found in the Supporting Information.

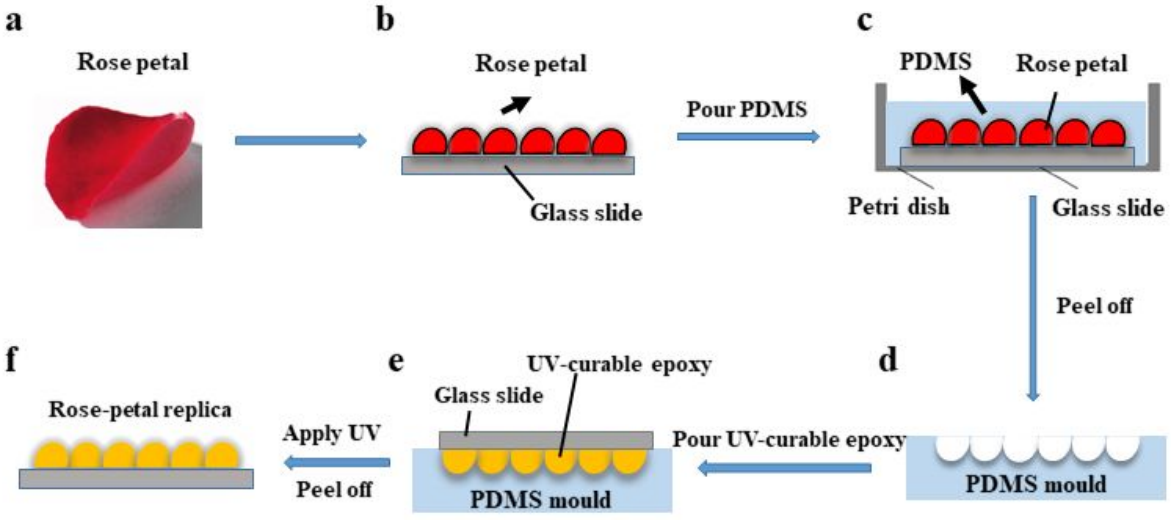

Figure 1. Schematic of the fabrication method to obtain rose-petal replicas.

2.2 Characterization of rose-petal structured surfaces: The replicas of rose-petal surfaces were imaged using a scanning electron microscope (SEM). FEI Helios NanoLab 600 DualBeam system was operated at an acceleration voltage of 5 KV, which allowed to get good magnifications, while will not damage the surfaces. We also measured the contact angles (CA) on flat and rose-petal-structured epoxy surfaces by placing a sessile drop of 3 µl deionized water (i.e. DI water), and evaluated by a CAM 100 optical contact angle meter (KSV Instruments Ltd., Finland). To characterize the evaporation dynamics, a 3 µl DI water droplet was placed on either of the surfaces, and their intensity projections were captured every 300 seconds by the optical contact angle meter. The droplet edges were extracted by an in-house Matlab code and plotted in a single image to visualize the droplet transitions overtime. An in-house goniometer[45-46] was set-up to measure the advancing contact angles on flat and rose-petal surfaces using a syringe-pump system (needle gauge ~25, water droplet volume ~10 µl, dispensing rate~ 0.2 ml/minute). Receding contact angles were also measured using the same method with the syringe pump operating in withdrawal mode. All the measurements were

repeated for three instances and the images were processed using ImageJ. Results are presented as the mean contact angles with standard deviations.

2.3 Bacteria culture, attachment and biofilm growth: Biofilm-forming strains of *S. epidermidis* FH8 and *P. aeruginosa* PAO1-mCherry were used in this study[47-49]. *S. epidermidis* FH8 was isolated from a chronic rhinosinusitis patient at the Freeman Hospital, Newcastle Upon Tyne[49]. PAO1-mCherry is the derivative of *P. aeruginosa* PAO1-N (Nottingham subline[50]), which was engineered via chromosomal insertion (attTn7::ptac-mcherry) to constitutively express a red fluorescent protein mCherry. *S. epidermidis* FH8 and *P. aeruginosa* PAO1-mCherry were routinely cultured in Tryptic Soy Broth (TSB, Melford Laboratories Ltd, UK), in an incubating shaker at 180 rpm, 37℃ for 16 hours and then used for experiments.

The optical density of *S. epidermidis* FH8 was measured by a spectrophotometer (Biochrom Libra S11, Biochrom Ltd., Cambridge, UK) and diluted to OD_{600}= 0.30 with fresh TSB medium. 3 ml of the diluted bacterial culture was incubated with flat and rose-petal structured surfaces in 12-well culture plates for 2 hours at 37℃ and then removed for visualization. To monitor the early-stage biofilm formation, we cultured *Staphylococcus epidermidis* FH8 on flat/rose-petal surfaces for up to 2 days. *P. aeruginosa* PAO1-mCherry colonizes surfaces rapidly. Therefore, to avoid overloading the system, different culture conditions were selected for *P. aeruginosa* with a lower bacterial inoculum (OD_{600}= 0.01) and incubation in 100x diluted TSB for 2 hours (bacterial attachment assay) or 24 hours (biofilm formation assay) . This method enabled biofilm growth to be visualised on the different surfaces without shielding the initial surface structure.

2.4 Fluorescent Microscope Analysis: After the bacterial attachment assay or biofilm formation assay, surfaces were gently rinsed three times with Phosphate Buffered Saline (PBS, pH=7.4) to remove loosely adhered bacteria. Surfaces incubated with PAO1-mCherry were directly visualized by fluorescent microscopy after washing. For *S. epidermidis* FH8, the adherent bacteria or biofilms were stained with SYTO®9 (Invitrogen, Life Technologies, Carlsbad, CA, USA) following the standardized methods. All surfaces were visualized using an Olympus BX61 upright fluorescent microscope with a 20x objective. For the bacterial attachment assay (2 hours), surfaces were examined (see Support Information) by acquiring 2D fluorescent images in a single focal plane (121.25 × 108.75 μm^2). For biofilms, z-stacks were performed through the thickness of biofilms from 5 random locations on the surfaces. The biomass in each field of view (430.00 × 324.38 μm^2) was determined using the COMSTAT2

plugin (Lyngby, Denmark) in ImageJ. Three independent experiments were performed for each surface type.

2.5 SEM Analysis: Surfaces (with bacteria or biofilms) were washed three times with PBS and fixed in 2% glutaraldehyde with 3M Sorenson's phosphate buffer, overnight at 4°C. Then they were dehydrated through a series of ethanol solutions of 25% (v/v), 50%, 75%, and 100%, followed by critical point drying (Leica EM CPD300). The dried surfaces (with bacteria or biofilms) were sputter-coated with 16 nm platinum to increase the surface conductivity, enabling higher resolution imaging by the SEM.

2.6 Statistical Analysis: Data are represented as mean values with standard error. Student's t-test assuming unequal variations was applied and $*p < 0.05$ was considered statistically significant in this study.

3. RESULTS AND DISCUSSION

3.1 Characterization of surface topography and wettability of rose-petal replicas

SEM imaging of the UV-epoxy rose-petal replicas (Figure 2 a1) revealed the existence of periodic arrays of hemispherical micro-papillae in the diameter of 23 ±3 μm , similar to the microstructures on natural rose petals (~ 20 μm)[43-44]. The magnified SEM images in Figure 2 a2 shows the existence of cuticular folds were found at the top of micro-papillae, closely mirroring the hierarchical topographies of the natural rose petal. The width of each fold was measured to be in the range of 700 ±100 nm, similar to the size as previously reported (~ 730 nm[43-44]) and the gap between each fold was measured to be 500 ±150 nm (Figure 2 a3). Collectively, the rose-petal replicas exhibit as hierarchical structures with micro-papillae and nano-folds in two different scales.

The static water contact angle (CA) on the flat surface was measured to be 60.5º ±6.5º (Figure 2b), indicating that the cured flat epoxy surface was intrinsically hydrophilic. For the rose-petal replicas, the CA value on surfaces was measured to be 130.8º ±4.3º (Figure 2b), indicating that the hierarchical structures had enhanced the surface hydrophobicity significantly. The water droplets stayed pinned on rose-petal structured surfaces under different tilt angles ranging from 30 - 180° (Figure 2c), implying that there exist highly adhesive interactions between the drops and the structured surfaces[43-44]. Contact angle hysteresis (CAH) measurement which is an indicator of slipperiness (water-repellence), were conducted by using the dynamic CA method

(by increasing or decreasing the volumes of water droplets using a needle[51]). CAH (also defined as the difference between the advancing and receding angle of a water droplet) of the rose-petal structured surfaces (91.0° ±4.9°) was measured to be significantly higher than that of the flat surfaces (44.8° ±4.3°), as shown in Figure 2b. This indicates the presence of a large number of pinning points on rose-petal structured surfaces, which cause the adhesion of liquid droplets.

We also evaluated the evaporation dynamics of water droplets on these two surfaces (Figure 2d), as CAH has been attributed to be the main factor affecting drop evaporation[52]. Figure e-f shows the evolution of CA and contact radius of a water droplet during the evaporation process. For the flat surface, the evaporation started with the constant contact line (CCL) mode up to 900s (Figure f): the CA decreased, while the contact radius remained constant. After that, the CA decreased to its receding CA (i.e. 37.6° ± 4.5° in this study), and contact line started to recede. The CA remained almost constant ranging from 900-1500s (Figure e), indicating that this is the constant contact angle (CCA) mode during this period of time. At the end of evaporation (1500-1800s), both CA and contact radius decreased (i.e. mixed mode) as shown in Figure f. This observation was consistent with the normal evaporation process which was reported on smooth hydrophilic surfaces[53]. By contrast, rose-petal structured surfaces exhibited mostly as CCL mode over time (Figure d &f & S1) due to its higher CAH. The CA of rose-petal surfaces require more time to decrease to its receding CA (i.e. 37.2° ± 4.3° in this study). Therefore, the contact line is pinned and contact radius keeps constant during the evaporation.

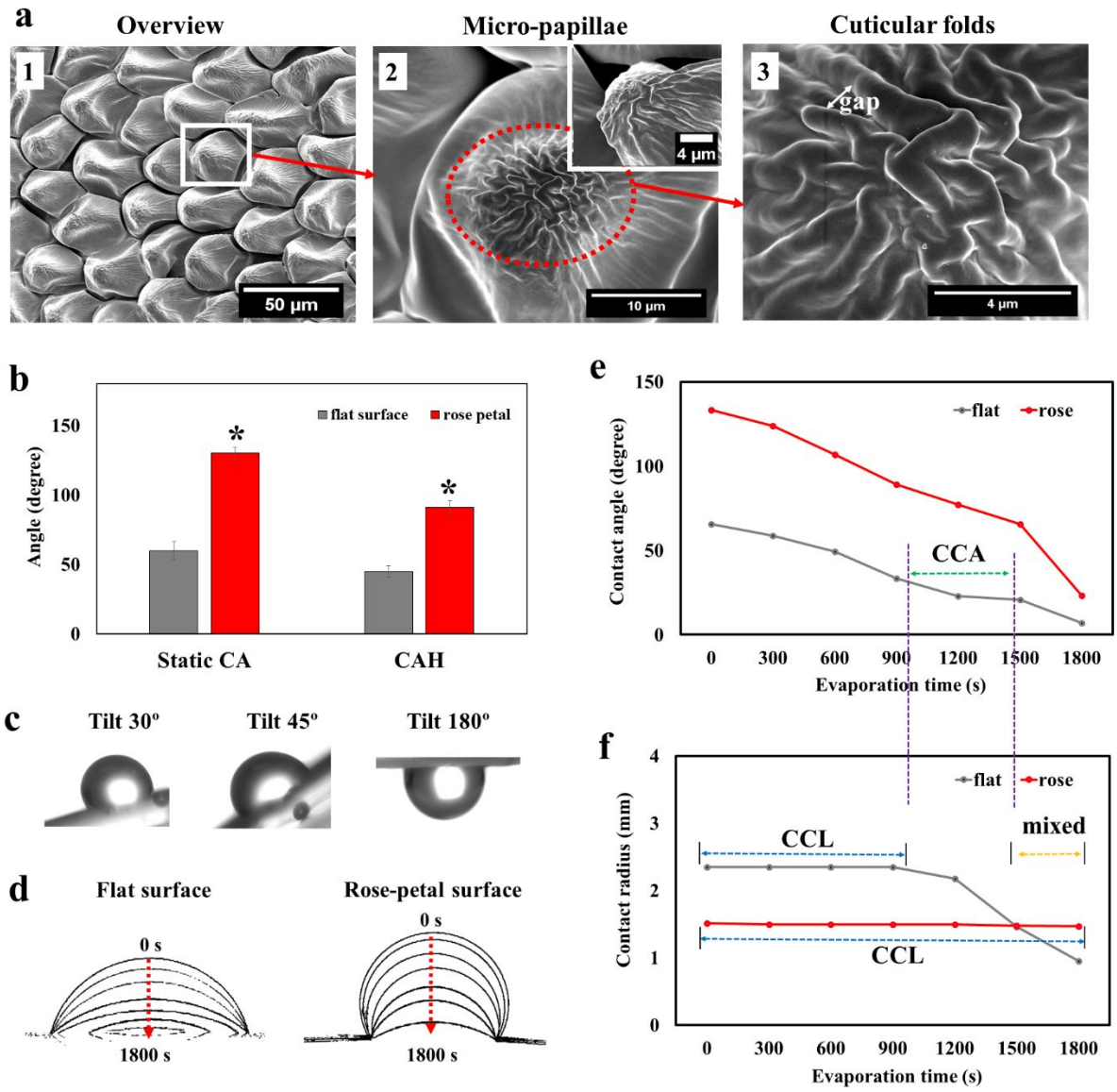

Figure 2. (a) SEM images of the rose-petal replicas made by UV-epoxy. (a1) an overview of the hierarchical structures on surface, taken at 1000x. (a2) A typical SEM image taken at 8000x showing the hemispherical micro-papillae with cuticular folds, and the inset was taken at 20° tilt with the magnification of 12000x. (a3) The magnified SEM image taken at 25000x showing the detailed cuticular nano-folds. **(b)** Static water contact angle (CA) and contact angle hysteresis (CAH) measurements on flat and rose-petal structured surfaces, $*p=6.7\times10^{-6}$ for CA and $*p=2.0\times10^{-13}$ for CAH. **(c)** Digital images of 3 μl water droplets on the rose-petal structured surfaces under different tilt angles. **(d)** A typical example of the edges of 3 μl water droplets, when evaporated on the flat and rose-petal structured surfaces overtime. The outside of droplet edge was extracted at the time of 0 s, and the time interval between each edge was 300 s. **(e-f)**

Evolution of contact angle (f) and contact radius (g) of water droplets (3 µl) evaporating on flat and rose-petal structured surfaces.

The evaporation process on rose-petal replicas didn't agree with the normal observations of hydrophobic surfaces, which is dominated by CCA mode as previously reported[52-53]. The normal hydrophobic or superhydrophobic surface like lotus leaf allows air to remain inside the texture (i.e. Cassie state), thereby have a low CAH. This results in the evaporation process follows as CCA mode with the easy receding of contact line[53]. However, it is believed that there have the coexistence of air pockets and water–solid contacts on rose-petal surface. This results in Cassie and Wenzel states coexist on rose-petal-like surfaces (also known as Cassie-Baxter impregnating wetting state[43-44]). Therefore, rose-petal surface is hydrophobic but have a high CAH[54]. This special wetting state is attributed to the hierarchical micro- (i.e. arrays of papillae) and nanostructures (i.e. cuticular folds) on rose-petal surface. The relatively large and periodic arrays of papillae can exert a capillary force that facilitates the penetration of water into papillae valleys[55]. However, the water cannot enter into the nanoscale structures (i.e. cuticular folds) at the top where tapped air pockets exist. This kind of special wetting state on the rose-petal surfaces is also termed as the "petal effect" and has been well investigated by researchers[43-44, 55].

3.2 Bacterial adherence is delayed by the rose-petal structured surfaces

We initially assessed the attachment of two common human pathogens, *S. epidermidis* (spherical-shape) and *P. aeruginosa* (rod-shape) on the different surfaces after 2 hours. A standard practice for counting planktonic cells is measuring colony forming units (CFU)[56]. However, this is not straightforward for enumeration of bacteria in biofilms on patterned surfaces owing to difficulties of removing all cells from the surface and breaking up aggregates into single cells without killing them[5, 56]. Therefore, fluorescence microscopy and quantitative image analysis was employed to enumerate bacterial cells in biofilms and to assess their distributions on the surface.

The distribution of fluorescence signals (green for *S. epidermidis* and red for *P. aeruginosa*) was relatively uniform on the flat surfaces, indicating that the bacterial cells had attached uniformly across the surface (Figure 3 a1&3). However in the case of rose-petal structured surfaces, the fluorescent patches of *S. epidermidis* or *P. aeruginosa* were sparsely scattered, and large areas without fluorescent signal were observed. This indicated that cells were only

able to attach to specific regions on the rose-petal structure (Figure 3 a2&4). Figure 3b shows that the surface area covered by *S. epidermidis* and *P. aeruginosa* on rose-petal structured surface, which was significantly lower (86.1± 6.2% less and 85.9 ±3.2% less, respectively) in comparison to the area covered by bacteria on flat surfaces. It is possible that the wash steps passing through the air-liquid interfaces may have selectively removed relatively weakly attached cells and affected the distribution of cells on surfaces[57]. Therefore, control experiments were performed where samples were never passed through an air-water interface and were imaged using a water dipping lens. The distribution of cells was very similar to those seen in washed samples (data not shown), indicating that forces exerted during wash steps do not have a major impact on attached bacterial cells. Overall, the observations indicate that the rose-petal structures have the ability to inhibit the initial bacterial attachment.

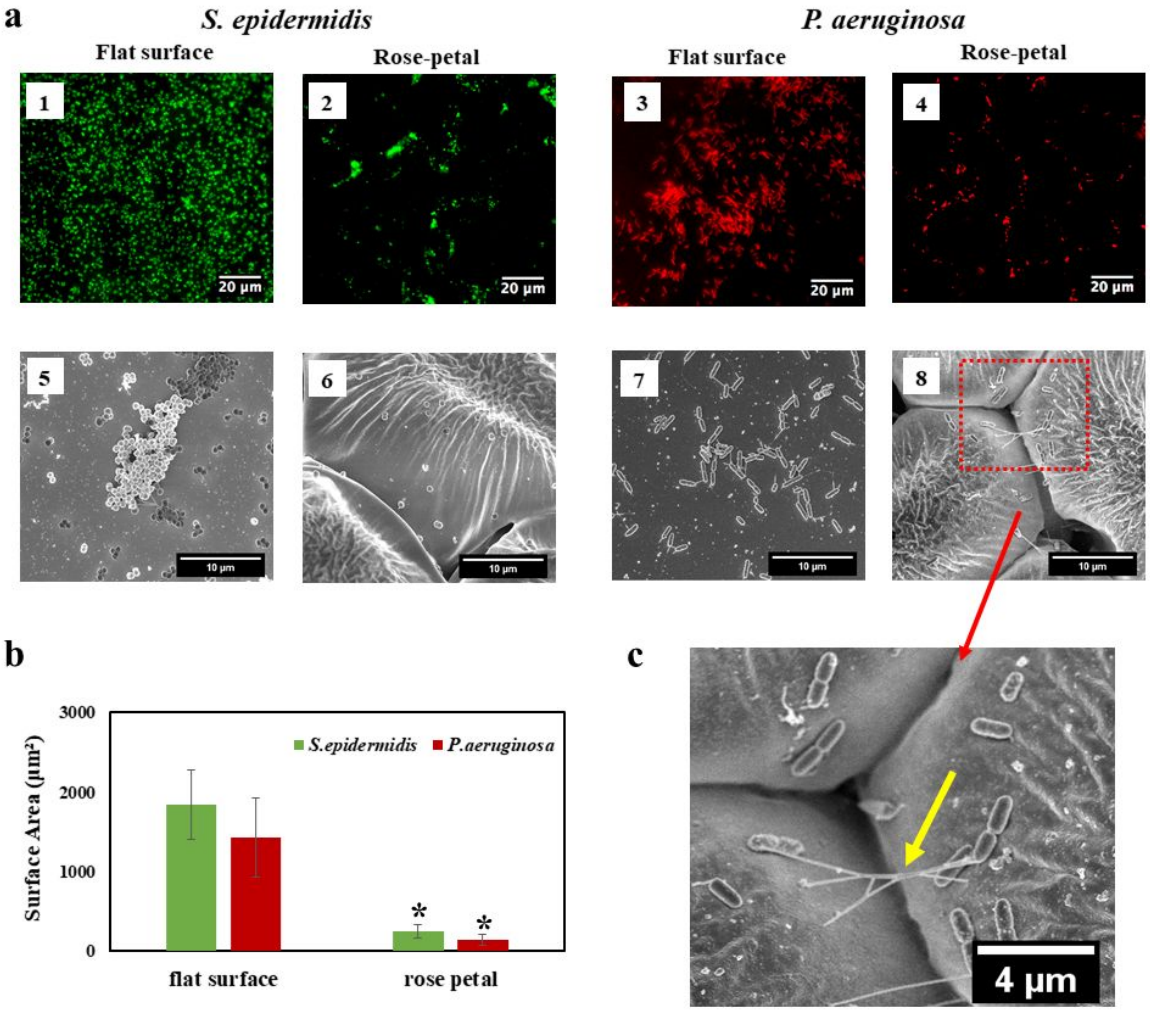

Figure 3. Adherence of *S. epidermidis* and *P. aeruginosa* on different surfaces after 2 hours' incubation. **(a)** Fluorescent microscopy (1-4) and SEM (5-8) images of *S. epidermidis* and *P. aeruginosa* on flat and rose-petal structured surfaces. **(b)** The surface area coverage of each

type of bacteria in the field of view (121.25 × 108.75 μm^2) for each surface was determined by ImageJ. *p=2.1×10^{-9} for *S. epidermidis* and *p=5.1×10^{-11} for *P. aeruginosa*. **(c)** A zoomed in view of the cross-section in a8 showed the existence of cellular appendages (yellow arrow), which might mediate bacterial attachment of *P. aeruginosa*, by connecting isolated cells.

To investigate the interactions at a higher spatial resolution, SEM was used to visualize *S. epidermidis/ P. aeruginosa* on different surfaces. On flat surfaces, *S. epidermidis* tended to cluster into small aggregates (Figure 3 a5). By contrast, on the rose-petal surfaces, which comprised of hierarchically arranged micro- (i.e. arrays of papillae) and nanostructures (i.e. cuticular folds), 85.6 ±5.8% of *S. epidermidis* cells (based on SEM images, n=9) were localized in the valleys or crevices between micro-papillae (Figure 3 a6 & S2). Cells were not commonly seen at the top of the micro-papillae. These observations were consistent with the acquired fluorescent images (Figure 3 a2&4), where large areas without fluorescent cells were seen and presumably represented the sites of nano-folds. We did not observe cell aggregates of *S. epidermidis* on rose-petal surface and found that most of the attached cells were isolated (Figure 3 a6 & S2). Similar observations were also found for *P. aeruginosa*, as shown in Figure 3 a7-8 & S3. In this case, 90.4 ±3.1% of cells (based on SEM images, n=9) were present in the valleys. The major difference between the cell types was that *P. aeruginosa* cells were connected by long tube-like appendages, which may have mediated cellular attachment by connecting the isolated cells together (Figure 3c).

3.3 Biofilm growth is delayed by the rose-petal structured surfaces

3.3.1 Biofilm growth of *S. epidermidis* on different surfaces

To investigate whether the rose-petal structures are effective in delaying biofilm growth, *S. epidermidis* biofilms were cultured for 2 days and then analysed using fluorescent microscopy as well as SEM (Figure 4). Maximum intensity projections through the thickness of *S. epidermidis* biofilms showed bright patches on the flat surface (Figure 4 a1), indicating a typical biofilm growth comprising multiple layers of cells. Few smaller green patches were observed on the rose-petal structured surface, which appeared as circular or oval structures with centrally located dark regions that lacked fluorescence (Figure 4 a2). The diameter of these circular regions were measured to be 21 ± 4 μm, which is similar to the dimensions of hemispherical micro-papillae (i.e. 23 ± 3 μm in diameter) on the rose-petal structures. This indicates that *S. epidermidis* clusters/biofilms preferentially form around the micro-papillae.

The total biomass on the rose-petal surface was significantly lower (63.2 ±9.4% less) compared with the biomass on the flat surface (see Figure 4c), indicating that rose-petal structure can delay the biofilm growth. A dense biofilm network was observed on the flat surface, and string-like structures consisting of filamentous fibrils appeared to bridge *S. epidermidis* cells together (Figure 4 b1&2). These filamentous fibrils are known to be part of EPS structure of *S. epidermidis* biofilms[58] which indicates a more mature biofilm growth. By contrast, no filamentous fibrils were observed on the rose-petal surfaces (Figure 4 b3&4). A few cellular clusters were sparsely scattered on the rose-petal structure and the majority of cells occupied the valleys between the micro-papillae (Figure 4 b3 & S4), consistent with the findings of fluorescent imaging (Figure 4 a2) which revealed cells preferentially surrounding the micro-papillae. Small aggregates of around ~20 cells were observed on the cuticular folds (Figure 4 b4), however 3D clusters or aggregates on the cuticular folds at the top of micro-papillae were relatively rare. The diameter of *S. epidermidis* cells were measured to be 700 ±70 nm in this study, which is of similar dimensions compared to the feature size of folds (width ~700 ±100 nm, gap ~500 ±150 nm). *S. epidermidis* cells can deposit into these fold gaps thereby forming small aggregates at the top of micro-papillae over time (Figure S4).

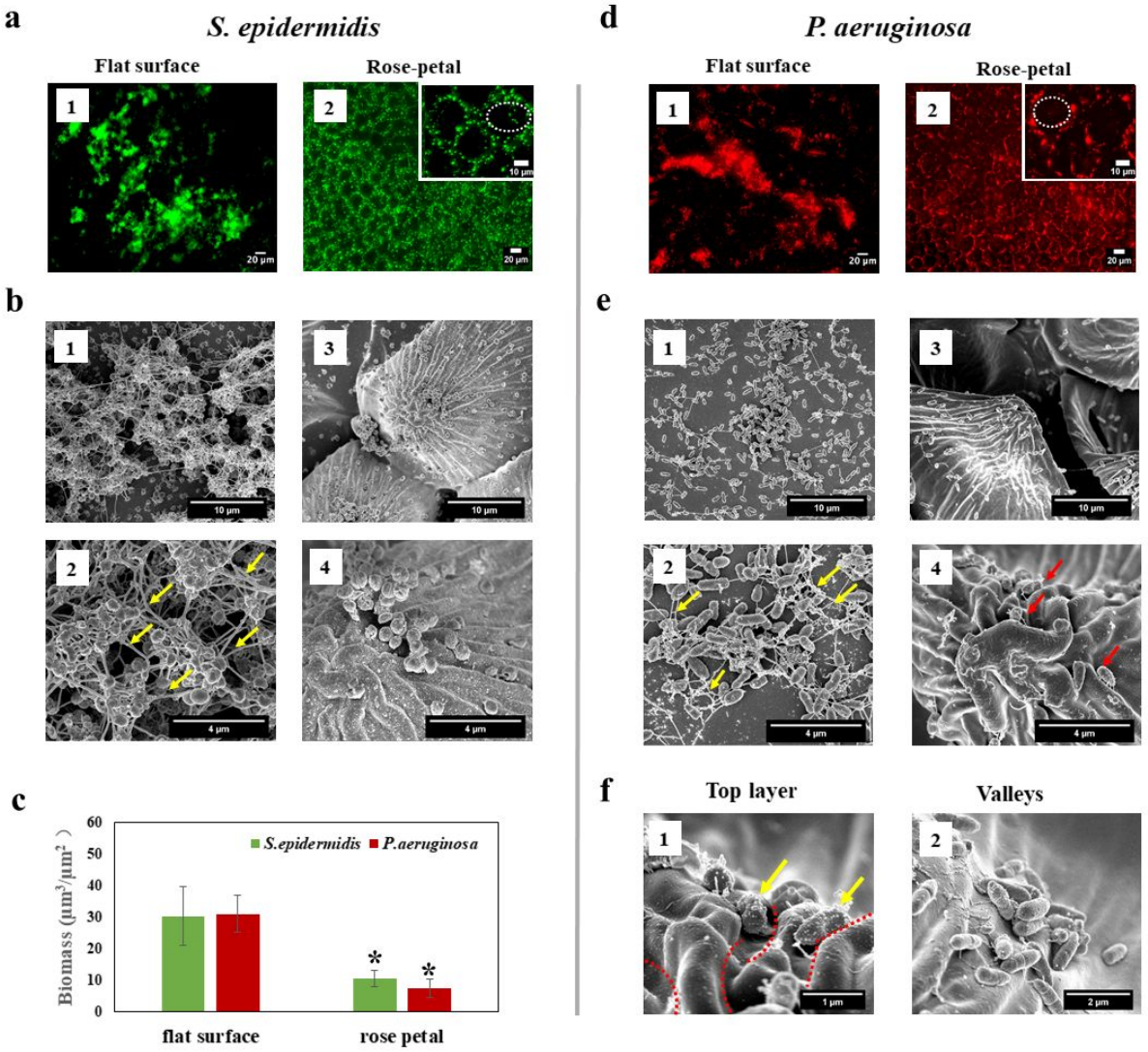

Figure 4. Biofilm formation (2 days) on the flat and rose-petal structured surfaces. **(a)** Fluorescent images of *S. epidermidis* biofilms on different surfaces. The cells on the rose-petal surfaces are distributed in oval shaped patterns which is highlighted by a dashed white line in a2. **(b)** SEM images of *S. epidermidis* biofilms on different surfaces. b1 and b3 are lower magnification images; b2 and b4 are high magnifications. Yellow arrows indicate the filamentous fibrils from the EPS of biofilms. **(c)** Biomass volume per unit area on the different surfaces calculated from ImageJ Comstat2. $*p=1.8\times10^{-6}$ for *S. epidermidis* and $*p=3.8\times10^{-11}$ for *P. aeruginosa*. **(d)** Fluorescent images showing *P. aeruginosa* biofilms on different surfaces. The dashed white line highlights a cuticular region, with cells distributed in a circular pattern around the edge of micro-papillae. **(e)** SEM images of *P. aeruginosa* biofilms on different surfaces at lower magnifications (e1 and e3) and higher magnifications (e2 and e4). Yellow arrows indicate the filamentous fibrils from the EPS of biofilms and red arrows indicate the isolated bacterial cells within the cuticular folds. **(f)** High-magnification SEM images of *P.*

aeruginosa biofilms on rose-petal surface, yellow arrows indicate the bacterial alignment within the cuticular nano-folds, and red dash lines indicate the boundary of folds, as shown in f1. *P. aeruginosa* aggregates can form in the valleys of micro-papillae, as shown in f2.

3.3.2 Biofilm growth of *P. aeruginosa* on different surfaces

Maximum intensity projections through the thickness of *P. aeruginosa* biofilms and the corresponding SEM images of the different surfaces are shown in Figure 4 d-e. Circular or oval shaped structures were observed in the fluorescent images of rose-petal surface (Figure 4 a4). This indicates that *P. aeruginosa* biofilm preferentially grew in between micro-papillae, akin to the growth mechanism of *S. epidermidis*. The total biomass of *P. aeruginosa* biofilms was significantly reduced on the rose-petal structured surfaces (76.0 ±10.0% less), comparing to the biomass on the flat surface (see Figure 4c). Figure 4e (1&2) shows the existence of *P. aeruginosa* clusters with a developed network of filamentous fibrils surrounding the cell bodies on the flat surface. In contrast to *S. epidermidis*, *P. aeruginosa* biofilms did not contain significant aggregates or clusters on the rose-petal surface, possibly due to the lower initial bacterial density and the nutrient-limited conditions arising from rapid cellular growth (Figure 4e 3 & S5). Most cells were found to be isolated on structured surfaces, in contrast to the flat surface (Figure 4e). At a higher magnification, small bacterial aggregates were observed, comprising ~10 cells in the valleys of micro-papillae on the rose-petal surface (Figure 4f 2 & S5 b), without showing the long filamentous fibrils. *P. aeruginosa* cells were also occasionally found attached within the cuticular nano-folds at the top of micro-papillae (Figure 4 e4& f1). We measured the gap between folds to be 500 ±150 nm (Figure 2 a3) which is similar to the diameter of *P. aeruginosa* and found that a single *P. aeruginosa* cell was capable of settling into these gaps over time. The cells tended to align with the folds (Figure 4 f1 & S5 c-d) and the preference for alignment along the nano-folds was strong even though the fold structure was irregular. The crowns of the cuticular folds were visible after the long-term bacterial growth (i.e. 24 hours), as the bacteria tended to remain confined in the ridges between the nano-folds (Figure 4 f1 & S5 c-d). To further assess *P. aeruginosa* biofilm growth, the period of biofilm development was extended to 48 hours - the same incubation time of *S. epidermidis* biofilms. In these experiments, the biomass on rose-petal structured surface was also found to be significantly lower (68.7 ± 13.4% less) in comparison of the biomass on the flat surface (Figure S5). The observations confirm that the rose-petal structure was able to delay the early stage biofilm growth of *P. aeruginosa*.

3.4 Bacterial growth of *P. aeruginosa* on unitary nano-pillars

We used a simpler surface pattern containing unitary nano-pillars to examine the alignment of *P. aeruginosa* and evaluate anti-microbial performance against the hierarchical rose-petal structures. The unitary nano-pillar structured surface was moderately hydrophobic (CA of 94.8°±3.7°) and the dimensions of the topographical features was similar to the nano-folds on rose-petals and comparable to the size of *P. aeruginosa* cells. Figure 5a and b1 showed that bacterial cells aligned with gaps between the nano-pillars after 2 hours, consistent with previous investigations[39]. Bacterial appendages tended to link to pillars (Figure 5b2). The total surface area covered by bacteria after 2 hours was significantly lower on the nano-pillar surface compared with the rose-petal surface (see Figure 5c&3b, 107.2±28.6 μm^2 vs 143.8±71.2 μm^2, p=0.012), possibly owing to the restricted area (pillar pitch) where bacteria can make the initial contacts to material surface. However, the biomass of *P. aeruginosa* after 24 hours (15.7±4.3 $\mu m^3/\mu m^2$, Figure 5c) on nano-pillars was significantly higher than on rose-petal replica surfaces (7.3±2.8 $\mu m^3/\mu m^2$, Figure 4c) (p=0.002). Bacteria continued to deposit into the nanopillar pitches, and dense filamentous fibrils were observed surrounding the cells, similar to the flat surfaces (Figure 5d2 and S7). However, the biomass on nano-pillars after 24 hours is still significant lower comparing to that on the flat surfaces (31.1±6.0 $\mu m^3/\mu m^2$, Figure 4c) (p= 2.7×10^{-7}), indicating that unitary nanostructures can still isolate cells and delay biofilm growth.

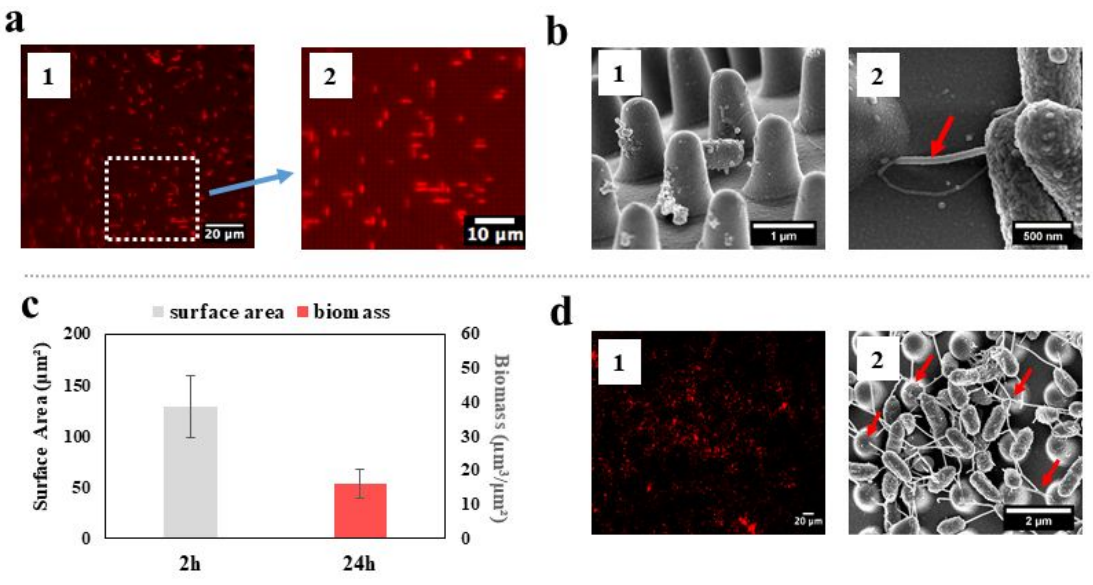

Figure 5. (a) Fluorescent microscopy and **(b)** SEM images of *P. aeruginosa* on nano-pillar surfaces after 2 hours, showing the cell patterning/aligning behaviour and a structure emanating from a bacterial cell (red arrow). **(c)** The surface area coverage (2 hours) and biomass (24 hours) of *P. aeruginosa* on nano-pillar surfaces. **(d)** Fluorescent microscopy and SEM images of *P.*

aeruginosa on nano-pillar surfaces after 24 hours, showing dense filamentous networks (red arrows).

3.5 The mechanism of inhibiting biofilm growth on rose-petal surface

The efficiency of bacterial attachment on surfaces is dictated by chemical and physical properties of surfaces[1]. We fabricated flat, rose-petal and nano-pillar structured surfaces using a nanocasting technique with UV-curable epoxy, so the surface chemistry in each case can be assumed to be the same. The major difference was the surface topographical features and this was a critical determinant of bacterial attachment and biofilm growth.

We hypothesized that hierarchical structures (i.e. micro-papillae and nano-folds) on rose-petal surfaces inhibit initial bacterial attachment after 2 hours. As a result of these structures, the rose petal surface exhibits as a modified state of hydrophobicity, termed as the Cassie-Baxter impregnating wetting state. The nanostructured cuticular folds can trap air within the folds, corresponding to the Cassie-state of lotus-leaf; thereby bacterial cells cannot penetrate the air-layer over short timeframes (Figure 6). This mechanism is similar to the lotus-leaf where the trapped air restricts the direct contact between bacteria and surfaces. However, unlike the lotus-leaf that has a low CAH, the papillae valleys can trap water thereby resulting in a high CAH. Visualizing the bacteria-material interfaces under the Cassie impregnating wetting state which combines wetting and non-wetting, is not an easy task. It may require sophisticated imaging such as high-resolution Cryo FIB-SEM instead of conventional microscopy[59], especially down to the 1µm scale. However, as seen in Figure 3, cells only preferentially colonize the valleys surrounding the papillae and this region is also devoid of nano-folds. The hypothesis which describes the lack of bacterial attachment within nano-folds (Figure 6) is consistent with our observation of *S. epidermidis* and *P. aeruginosa* adherence behaviour on rose petal surfaces (~2 hours).

If the bacterial growth extends to 1-2 days (biofilm assay), bacterial cells still only accumulate surrounding the papillae forming ring/oval-like structures (Figure 6). The initial wetted micro-papillae valleys can harbour more bacterial cells as they tend to increase the overall surface area, thereby are more favourable for cell colonization if comparing to the nano-folds (Figure 6). However, unlike biofilms spreading on the flat or unitary nano-pillar surfaces, we found that either *S. epidermidis* or *P. aeruginosa* biofilms on rose-petal surfaces were isolated and overall biofilm growth was impaired (Figure 4). Notably, we found that the bacterial growth

was lower on unitary nano-pillars after 2 hours, whilst biofilm formation was increased after 24 hours if comparing with the rose-petal surfaces. On unitary nano-pillars, the fibres produced by bacteria established connections between isolated cells, and thus may mediate cell-cell communication (Figure S7). However, no large bacterial clusters or dense filamentous structures were found within micro-papillae on rose-petal surfaces (Figure 4). The papillae depth may play an important role as a physical barrier to hinder the development of fibrous network. Therefore, the communication between the neighbouring cell aggregates/clusters that self-developed in each papillae valley may get blocked, and consequently retard biofilm development (Figure 6). Such a hindrance of biofilm development by specific topographically engineered surfaces has been observed previously[7, 60-61]. For example, colloidal crystals of a larger diameter (~1500 nm) can more effectively separate cell bodies than the ones in a diameter of 450 nm, thereby delaying biofilm growth[60]. Other studies have tested biofilm growth on micro-posts (~20×20 µm, pitch~10 µm), similar to the dimension of micro-papillae on the rose-petals[61]. Decreased biofilm growth was observed within the valleys between the unitary micro-posts, while more biofilm was formed on the top of posts (i.e. protruding plateaus)[61]. This indicated that a larger scaled topography size helps to isolate cells while its larger contact area on the top may facilitate more bacterial growth.

However, no significant clusters within nano-folds were found, indicating that creating a secondary topography on the microstructure is more effective to delay bacterial growth compared with the bare microstructures. When submerged in water, the trapped air in nano-folds would vanish over time, similar to the lotus-leaf structures, resulting in the transition of Cassie to Wenzel state. Bacterial cells can eventually make contacts with the nano-folds after this region is completely wetted (Figure 6). The dimensions of nano-folds (width ~700 ±100 nm, gap ~500 ±150 nm) are similar to the bacterial size. Therefore, either *S. epidermidis* or *P. aeruginosa* cells can deposit into the folds and align with the fold structure, especially for *P. aeruginosa* (Figure 4& 6). *P. aeruginosa* cells also align within unitary nano-pillars (Figure 5), which maximizes the contact area with the material surfaces. Similar observations have been reported by other researchers, although the underpinning mechanism is not yet clear[10, 62-64]. Specific bacterial mutants could be a useful tool to investigate cell alignment and surface structure mediated cell-cell communication, and this will be a target for future work. However, the long and irregular fold ridges can isolate cells via the alignment on rose-petal (Figure S5c&6), and such isolation behaviour is also identical on our nano-pillars with showing the lower biofilm biomass comparing to the flat surfaces. This delayed the formation of cell-cell

connections, thereby hindering their communication and constraining bacterial cluster development.

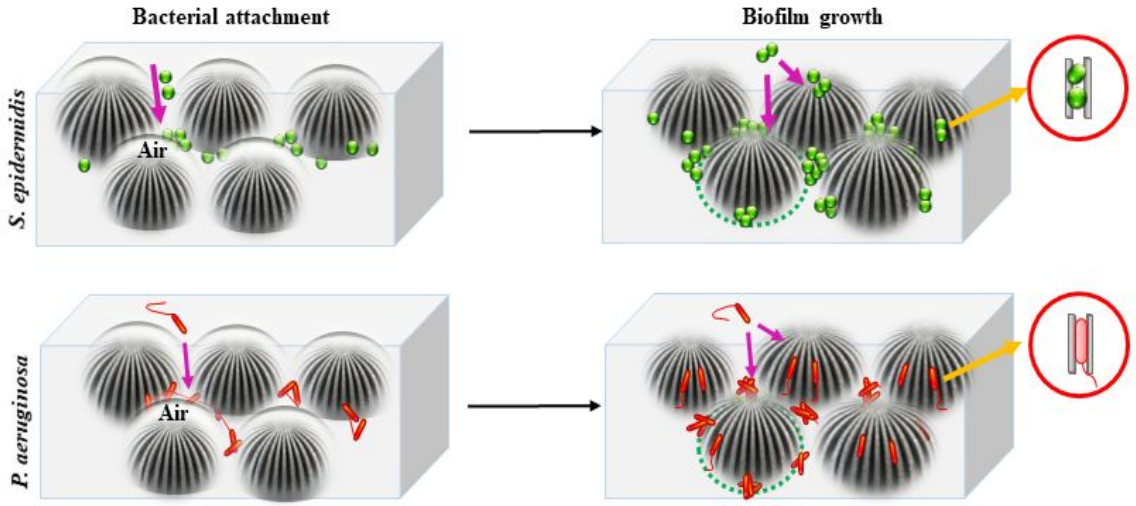

Figure 6. Hypothesized anti-biofilm mechanisms for the transition from bacterial attachment to biofilm growth on rose petal structured surfaces.

CONCLUSIONS

In summary, our study has revealed that rose-petal structured surfaces can delay bacterial attachment and biofilm formation with clinically relevant strains of bacteria. We successfully demonstrated the fabrication of a hierarchical rose-petal structure via a simple UV-curable nanocasting technique, which is cost-effective when compared with fabrication methods like e-beam lithography and nanoimprinting lithography. The rose-petal replicas exhibit a high CA and CAH as a Cassie impregnating wetting state. Similar to superhydrophobic lotus-leaf, the trapped air within nano-folds may hinder the bacterial attachment. While bacteria preferentially form clusters within the valleys of micro-papillae, as they are preferentially wetted and offer more favourable colonization sites when comparing to the nano-folds. We specifically discussed the anti-biofilm mechanism of hierarchical structures under submerged conditions, and the different topography size influence biofilm formation via different mechanisms: micro-papillae blocked the bacterial clusters in between the valleys, limiting the potential for cell-cell communication via fibrous networks, thereby resulting in impaired biofilm growth. At the same time, having a secondary nanostructure (nano-folds) on microstructures can align bacterial cells within the constrained gaps, thereby delaying in developing cell clusters during short term growth of biofilm.

Rose-petal surfaces have shown potential in parallel and multistep droplet manipulation owing to their high CAH. The hierarchical structures characterized here may be useful for the development of microfluidics and portable/wearable biosensors[65]. In addition, such hierarchical structures can capture and release circulating tumor cells (CTCs) for subsequent analysis[66], exhibiting great potential in biomedical devices. Therefore, this study is a significant step toward the application of rose-petal surfaces where biofilm control is also important. Furthermore, hierarchical structures may be useful to study the roles of microbial cell-cell interactions in biofilm formation. Determining the most effective topography size for controlling biofilm development is an important next step for the development of antifouling surfaces. Future studies will also aim to investigate the anti-biofilm mechanisms in more detail, for example by comparing the anti-biofilm efficacy of rose-petal hierarchical structures with other artificial unitary or hierarchical structures with different scales, investigating bacterial patterning on rose-petal nano-folds and their effects on biofilm formation, and determining whether rose petal replica surfaces are capable of inhibiting growth of biofilms by different species of bacteria.

AUTHOR INFORMATION

Corresponding Author

* *Jinju Chen: Email: jinju.chen@ncl.ac.uk*

Author Contributions

All authors contributed to this work. Y.C., S.J., N.R., J.B., H.L., N.J. and J.C. designed the research. Y.C., S.J., performed experiments and acquired the data, and performed the data analysis. L.B. and X.T. conducted the SEM experiments. Y.C., N.J. and J.C. prepared the original draft. All authors reviewed and edited the manuscript. All authors have given approval to the final version of the manuscript.

ACKNOWLEDGMENTS

Y. Cao acknowledges the PhD studentship (Research Excellence Academy funding scheme) from Newcastle University. J. Chen acknowledges funding from the Engineering and Physical Sciences Research Council (EP/K039083/1) and EPSRC Partnering for GCRF(EP/R512692/1). SJ acknowledges funding from Engineering and Physical Sciences Research Council

(EP/K039083/1). The authors are grateful for the technical support of Alex Laude from Bioimaging Facility, Newcastle University. We also acknowledge the technical assistance and useful discussions with Rebecca Jones and Ekaterina Kozhevnikova.

REFERENCES

1. Berne, C.; Ellison, C. K.; Ducret, A.; Brun, Y. V., Bacterial adhesion at the single-cell level. *Nature Reviews Microbiology* **2018,** *16*, 616-27.
2. Mon, H.; Chang, Y.-R.; Ritter, A. L.; Falkinham Iii, J. O.; Ducker, W. A., Effects of Colloidal Crystals, Antibiotics, and Surface-bound antimicrobials on Pseudomonas aeruginosa Surface Density. *ACS Biomaterials Science & Engineering* **2017,** *4* (1), 257-265.
3. Joo, H.-S.; Otto, M., Molecular basis of in vivo biofilm formation by bacterial pathogens. *Chemistry & biology* **2012,** *19* (12), 1503-1513.
4. Bryers, J. D., Medical biofilms. *Biotechnology and bioengineering* **2008,** *100* (1), 1-18.
5. Cao, Y.; Su, B.; Chinnaraj, S.; Jana, S.; Bowen, L.; Charlton, S.; Duan, P.; Jakubovics, N. S.; Chen, J., Nanostructured titanium surfaces exhibit recalcitrance towards Staphylococcus epidermidis biofilm formation. *Scientific reports* **2018,** *8* (1), 1071.
6. Mantle, S.; England, N. H. S., Reducing HCAI-What the Commissioner needs to know. *NHS England* **2015,** *8*.
7. Chang, Y.-R.; Weeks, E. R.; Ducker, W. A., Surface Topography Hinders Bacterial Surface Motility. *ACS applied materials & interfaces* **2018,** *10* (11), 9225-9234.
8. Mah, T.-F.; Pitts, B.; Pellock, B.; Walker, G. C.; Stewart, P. S.; O'Toole, G. A., A genetic basis for Pseudomonas aeruginosa biofilm antibiotic resistance. *Nature* **2003,** *426* (6964), 306.
9. Li, X.; Cheung, G. S.; Watson, G. S.; Watson, J. A.; Lin, S.; Schwarzkopf, L.; Green, D. W., The nanotipped hairs of gecko skin and biotemplated replicas impair and/or kill pathogenic bacteria with high efficiency. *Nanoscale* **2016**.
10. Friedlander, R. S.; Vlamakis, H.; Kim, P.; Khan, M.; Kolter, R.; Aizenberg, J., Bacterial flagella explore microscale hummocks and hollows to increase adhesion. *Proceedings of the National Academy of Sciences* **2013,** *110* (14), 5624-5629.
11. Saison, T.; Peroz, C.; Chauveau, V.; Berthier, S.; Sondergard, E.; Arribart, H., Replication of butterfly wing and natural lotus leaf structures by nanoimprint on silica sol–gel films. *Bioinspiration & biomimetics* **2008,** *3* (4), 046004.
12. Koch, K.; Bhushan, B.; Jung, Y. C.; Barthlott, W., Fabrication of artificial Lotus leaves and significance of hierarchical structure for superhydrophobicity and low adhesion. *Soft Matter* **2009,** *5* (7), 1386-1393.

13. Watson, G. S.; Green, D. W.; Cribb, B. W.; Brown, C. L.; Meritt, C. R.; Tobin, M. J.; Vongsvivut, J.; Sun, M.; Liang, A.-P.; Watson, J. A., Insect analogue to the Lotus leaf: a planthopper wing membrane incorporating a low-adhesion, nonwetting, superhydrophobic, bactericidal, and biocompatible surface. *ACS applied materials & interfaces* **2017,** *9* (28), 24381-24392.
14. Liu, Y.; Choi, C.-H., Condensation-induced wetting state and contact angle hysteresis on superhydrophobic lotus leaves. *Colloid and Polymer Science* **2013,** *291* (2), 437-445.
15. Kumar, C.; Le Houérou, V.; Speck, T.; Bohn, H. F., Straightforward and precise approach to replicate complex hierarchical structures from plant surfaces onto soft matter polymer. *Royal Society open science* **2018,** *5* (4), 172132.
16. Odom, T. W.; Love, J. C.; Wolfe, D. B.; Paul, K. E.; Whitesides, G. M., Improved pattern transfer in soft lithography using composite stamps. *Langmuir* **2002,** *18* (13), 5314-5320.
17. Wolfe, D. B.; Love, J. C.; Whitesides, G. M., Nanostructures replicated by polymer molding. *Encyclopedia of Nanoscience and Nanotechnology* **2004**.
18. Truong, V. K.; Webb, H. K.; Fadeeva, E.; Chichkov, B. N.; Wu, A. H. F.; Lamb, R.; Wang, J. Y.; Crawford, R. J.; Ivanova, E. P., Air-directed attachment of coccoid bacteria to the surface of superhydrophobic lotus-like titanium. *Biofouling* **2012,** *28* (6), 539-550.
19. Fadeeva, E.; Truong, V. K.; Stiesch, M.; Chichkov, B. N.; Crawford, R. J.; Wang, J.; Ivanova, E. P., Bacterial retention on superhydrophobic titanium surfaces fabricated by femtosecond laser ablation. *Langmuir* **2011,** *27* (6), 3012-3019.
20. Ma, J.; Sun, Y.; Gleichauf, K.; Lou, J.; Li, Q., Nanostructure on taro leaves resists fouling by colloids and bacteria under submerged conditions. *Langmuir* **2011,** *27* (16), 10035-10040.
21. Tang, P.; Zhang, W.; Wang, Y.; Zhang, B.; Wang, H.; Lin, C.; Zhang, L., Effect of superhydrophobic surface of titanium on staphylococcus aureus adhesion. *Journal of Nanomaterials* **2011,** *2011*, 2.
22. Crick, C. R.; Ismail, S.; Pratten, J.; Parkin, I. P., An investigation into bacterial attachment to an elastomeric superhydrophobic surface prepared via aerosol assisted deposition. *Thin Solid Films* **2011,** *519* (11), 3722-3727.
23. Zhang, X.; Wang, L.; Levänen, E., Superhydrophobic surfaces for the reduction of bacterial adhesion. *Rsc Advances* **2013,** *3* (30), 12003-12020.
24. Lee, C.; Kim, C.-J. C., Maximizing the giant liquid slip on superhydrophobic microstructures by nanostructuring their sidewalls. *Langmuir* **2009,** *25* (21), 12812-12818.
25. Bhushan, B.; Jung, Y. C.; Koch, K., Micro-, nano-and hierarchical structures for superhydrophobicity, self-cleaning and low adhesion. *Philosophical Transactions of the Royal Society A: Mathematical, Physical and Engineering Sciences* **2009,** *367* (1894), 1631-1672.

26. Kim, P.; Kreder, M. J.; Alvarenga, J.; Aizenberg, J., Hierarchical or not? Effect of the length scale and hierarchy of the surface roughness on omniphobicity of lubricant-infused substrates. *Nano letters* **2013,** *13* (4), 1793-1799.
27. Dai, S.; Zhang, D.; Shi, Q.; Han, X.; Wang, S.; Du, Z., Biomimetic fabrication and tunable wetting properties of three-dimensional hierarchical ZnO structures by combining soft lithography templated with lotus leaf and hydrothermal treatments. *CrystEngComm* **2013,** *15* (27), 5417-5424.
28. Lorenzetti, M.; Dogša, I.; Stošicki, T. a.; Stopar, D.; Kalin, M.; Kobe, S.; Novak, S. a., The influence of surface modification on bacterial adhesion to titanium-based substrates. *ACS applied materials & interfaces* **2015,** *7* (3), 1644-1651.
29. Bixler, G. D.; Theiss, A.; Bhushan, B.; Lee, S. C., Anti-fouling properties of microstructured surfaces bio-inspired by rice leaves and butterfly wings. *Journal of colloid and interface science* **2014,** *419*, 114-133.
30. Dundar Arisoy, F.; Kolewe, K. W.; Homyak, B.; Kurtz, I. S.; Schiffman, J. D.; Watkins, J. J., Bioinspired Photocatalytic Shark Skin Surfaces with Antibacterial and Antifouling Activity via Nanoimprint Lithography. *ACS applied materials & interfaces* **2018**.
31. Reddy, S. T.; Chung, K. K.; McDaniel, C. J.; Darouiche, R. O.; Landman, J.; Brennan, A. B., Micropatterned surfaces for reducing the risk of catheter-associated urinary tract infection: an in vitro study on the effect of sharklet micropatterned surfaces to inhibit bacterial colonization and migration of uropathogenic Escherichia coli. *Journal of endourology* **2011,** *25* (9), 1547-1552.
32. Chung, K. K.; Schumacher, J. F.; Sampson, E. M.; Burne, R. A.; Antonelli, P. J.; Brennan, A. B., Impact of engineered surface microtopography on biofilm formation of Staphylococcus aureus. *Biointerphases* **2007,** *2* (2), 89-94.
33. Green, D. W.; Lee, K. K.-H.; Watson, J. A.; Kim, H.-Y.; Yoon, K.-S.; Kim, E.-J.; Lee, J.-M.; Watson, G. S.; Jung, H.-S., High Quality Bioreplication of Intricate Nanostructures from a Fragile Gecko Skin Surface with Bactericidal Properties. *Scientific Reports* **2017,** *7*.
34. Watson, G. S.; Green, D. W.; Schwarzkopf, L.; Li, X.; Cribb, B. W.; Myhra, S.; Watson, J. A., A gecko skin micro/nano structure–A low adhesion, superhydrophobic, anti-wetting, self-cleaning, biocompatible, antibacterial surface. *Acta biomaterialia* **2015,** *21*, 109-122.
35. Diu, T.; Faruqui, N.; Sjostrom, T.; Lamarre, B.; Jenkinson, H. F.; Su, B.; Ryadnov, M. G., Cicada-inspired cell-instructive nanopatterned arrays. *Sci Rep* **2014,** *4*, 7122. DOI: 10.1038/srep07122.
36. Ivanova, E. P.; Hasan, J.; Webb, H. K.; Truong, V. K.; Watson, G. S.; Watson, J. A.; Baulin, V. A.; Pogodin, S.; Wang, J. Y.; Tobin, M. J.; Lobbe, C.; Crawford, R. J., Natural bactericidal surfaces: mechanical rupture of Pseudomonas aeruginosa cells by cicada wings. *Small* **2012,** *8* (16), 2489-94. DOI: 10.1002/smll.201200528.

37. Bhadra, C. M.; Truong, V. K.; Pham, V. T.; Al Kobaisi, M.; Seniutinas, G.; Wang, J. Y.; Juodkazis, S.; Crawford, R. J.; Ivanova, E. P., Antibacterial titanium nano-patterned arrays inspired by dragonfly wings. *Sci Rep* **2015,** *5*, 16817. DOI: 10.1038/srep16817.
38. Bandara, C. D.; Singh, S.; Afara, I. O.; Wolff, A.; Tesfamichael, T.; Ostrikov, K.; Oloyede, A., Bactericidal Effects of Natural Nanotopography of Dragonfly Wing on Escherichia coli. *ACS Applied Materials & Interfaces* **2017,** *9* (8), 6746-6760.
39. Hochbaum, A. I.; Aizenberg, J., Bacteria pattern spontaneously on periodic nanostructure arrays. **2010**.
40. Díaz, C.; Schilardi, P.; Salvarezza, R.; de Mele, M. F. L., Have flagella a preferred orientation during early stages of biofilm formation?: AFM study using patterned substrates. *Colloids and Surfaces B: Biointerfaces* **2011,** *82* (2), 536-542.
41. Hsu, L.; Fang, J.; Borca-Tasciuc, D.; Worobo, R.; Moraru, C. I., The effect of micro-and nanoscale topography on the adhesion of bacterial cells to solid surfaces. *Applied and environmental microbiology* **2013**, AEM. 03436-12.
42. Lai, C. Q., Bacterial Attachment, Aggregation, and Alignment on Subcellular Nanogratings. *Langmuir* **2018,** *34* (13), 4059-4070.
43. Feng, L.; Zhang, Y.; Xi, J.; Zhu, Y.; Wang, N.; Xia, F.; Jiang, L., Petal effect: a superhydrophobic state with high adhesive force. *Langmuir* **2008,** *24* (8), 4114-4119.
44. Dou, X.-Q.; Zhang, D.; Feng, C.; Jiang, L., Bioinspired hierarchical surface structures with tunable wettability for regulating bacteria adhesion. *ACS nano* **2015,** *9* (11), 10664-10672.
45. Gart, S.; Mates, J. E.; Megaridis, C. M.; Jung, S., Droplet impacting a cantilever: A leaf-raindrop system. *Physical Review Applied* **2015,** *3* (4), 044019.
46. Huhtamäki, T.; Tian, X.; Korhonen, J. T.; Ras, R. H., Surface-wetting characterization using contact-angle measurements. *Nature protocols* **2018,** *13* (7), 1521.
47. McFarland, K. A.; Dolben, E. L.; LeRoux, M.; Kambara, T. K.; Ramsey, K. M.; Kirkpatrick, R. L.; Mougous, J. D.; Hogan, D. A.; Dove, S. L., A self-lysis pathway that enhances the virulence of a pathogenic bacterium. *Proceedings of the National Academy of Sciences* **2015,** *112* (27), 8433-8438.
48. Weigert, M.; Ross-Gillespie, A.; Leinweber, A.; Pessi, G.; Brown, S. P.; Kümmerli, R., Manipulating virulence factor availability can have complex consequences for infections. *Evolutionary applications* **2017,** *10* (1), 91-101.
49. Shields, R. C.; Mokhtar, N.; Ford, M.; Hall, M. J.; Burgess, J. G.; ElBadawey, M. R.; Jakubovics, N. S., Efficacy of a marine bacterial nuclease against biofilm forming microorganisms isolated from chronic rhinosinusitis. *PLoS One* **2013,** *8* (2), e55339.
50. Sidorenko, J.; Jatsenko, T.; Kivisaar, M., Ongoing evolution of Pseudomonas aeruginosa PAO1 sublines complicates studies of DNA damage

repair and tolerance. *Mutation Research/Fundamental and Molecular Mechanisms of Mutagenesis* **2017,** *797*, 26-37.
51. MacCallum, N.; Howell, C.; Kim, P.; Sun, D.; Friedlander, R.; Ranisau, J.; Ahanotu, O.; Lin, J. J.; Vena, A.; Hatton, B., Liquid-infused silicone as a biofouling-free medical material. *ACS Biomaterials Science & Engineering* **2014,** *1* (1), 43-51.
52. Chuang, Y.-C.; Chu, C.-K.; Lin, S.-Y.; Chen, L.-J., Evaporation of water droplets on soft patterned surfaces. *Soft matter* **2014,** *10* (19), 3394-3403.
53. Khedir, K. R.; Kannarpady, G. K.; Ishihara, H.; Woo, J.; Trigwell, S.; Ryerson, C.; Biris, A. S., Advanced studies of water evaporation kinetics over teflon-coated tungsten nanorod surfaces with variable hydrophobicity and morphology. *The Journal of Physical Chemistry C* **2011,** *115* (28), 13804-13812.
54. Kulinich, S.; Farzaneh, M., Effect of contact angle hysteresis on water droplet evaporation from super-hydrophobic surfaces. *Applied Surface Science* **2009,** *255* (7), 4056-4060.
55. Shin, S.; Seo, J.; Han, H.; Kang, S.; Kim, H.; Lee, T., Bio-inspired extreme wetting surfaces for biomedical applications. *Materials* **2016,** *9* (2), 116.
56. Azeredo, J.; Azevedo, N. F.; Briandet, R.; Cerca, N.; Coenye, T.; Costa, A. R.; Desvaux, M.; Di Bonaventura, G.; Hébraud, M.; Jaglic, Z., Critical review on biofilm methods. *Critical reviews in microbiology* **2017,** *43* (3), 313-351.
57. Busscher, H. J.; van der Mei, H. C., Microbial adhesion in flow displacement systems. *Clinical microbiology reviews* **2006,** *19* (1), 127-141.
58. Takahashi, C.; Kalita, G.; Ogawa, N.; Moriguchi, K.; Tanemura, M.; Kawashima, Y.; Yamamoto, H., Electron microscopy of Staphylococcus epidermidis fibril and biofilm formation using image-enhancing ionic liquid. *Analytical and bioanalytical chemistry* **2015,** *407* (6), 1607-1613.
59. Rykaczewski, K.; Landin, T.; Walker, M. L.; Scott, J. H. J.; Varanasi, K. K., Direct imaging of complex nano-to microscale interfaces involving solid, liquid, and gas phases. *ACS nano* **2012,** *6* (10), 9326-9334.
60. Kargar, M.; Chang, Y.-R.; Khalili Hosseinabad, H.; Pruden, A.; Ducker, W. A., Colloidal Crystals Delay Formation of Early Stage Bacterial Biofilms. *ACS Biomaterials Science & Engineering* **2016**.
61. Hou, S.; Gu, H.; Smith, C.; Ren, D., Microtopographic patterns affect Escherichia coli biofilm formation on poly (dimethylsiloxane) surfaces. *Langmuir* **2011,** *27* (6), 2686-2691.
62. Dubey, G. P.; Mohan, G. B. M.; Dubrovsky, A.; Amen, T.; Tsipshtein, S.; Rouvinski, A.; Rosenberg, A.; Kaganovich, D.; Sherman, E.; Medalia, O., Architecture and characteristics of bacterial nanotubes. *Developmental cell* **2016,** *36* (4), 453-461.
63. Baidya, A. K.; Bhattacharya, S.; Dubey, G. P.; Mamou, G.; Ben-Yehuda, S., Bacterial nanotubes: a conduit for intercellular molecular trade. *Current opinion in microbiology* **2018,** *42*, 1-6.

64. Dubey, G. P.; Ben-Yehuda, S., Intercellular nanotubes mediate bacterial communication. *Cell* **2011,** *144* (4), 590-600.

65. Wong, W. S.; Nasiri, N.; Liu, G.; Rumsey-Hill, N.; Craig, V. S.; Nisbet, D. R.; Tricoli, A., Flexible transparent hierarchical nanomesh for rose petal - like droplet manipulation and lossless transfer. *Advanced Materials Interfaces* **2015,** *2* (9), 1500071.

66. Dou, X.; Li, P.; Jiang, S.; Bayat, H.; Schönherr, H., Bioinspired hierarchically structured surfaces for efficient capture and release of circulating tumor cells. *ACS applied materials & interfaces* **2017,** *9* (10), 8508-8518.

Table of Contents Graphic